Supplementary materials for

Exploring Polycrystalline Materials: High-throughput Phase Elucidation Using Serial Rotation Electron Diffraction

Yi Luo,[#†] Bin Wang,[#†] Stef Smeets,[‡] Junliang Sun,[≝] Weimin Yang,[§*] and Xiaodong Zou[†*]

[†]Department of Materials and Environmental Chemistry, Stockholm University, SE-106 91 Stockholm, Sweden.

[§]State Key Laboratory of Green Chemical Engineering and Industrial Catalysis, Sinopec Shanghai Research Institute of Petrochemical Technology, 1658 Pudong Beilu, Shanghai 201208, China.

[‡]Netherlands eScience Center, Science Park 140, 1098 XG Amsterdam, The Netherlands.

[≝]College of Chemistry and Molecular Engineering, Beijing National Laboratory for Molecular Sciences, Peking University, Beijing 100871, China.

[#]Y. Luo and B. Wang contributed equally to this work

Table of contents

Experimental Section

1. Experimental design

Massive studies have demonstrated that organic structure-directing agents (OSDAs) play a core role in the crystallization of zeolites. In recent years, the search for novel zeolite materials was driven by the design and synthesis of novel OSDAs, endowing them with larger sizes, unique conformations and compositions, and multi-function[1]. Large, bulky OSDAs usually show very strong structure-directing ability and dominate the crystallization process to form specific framework structures[2]. Many novel zeolites therefore have been synthesized using those large, bulky OSDAs. However, the preparation of the large, bulky OSDAs is always challenging, complex, and expensive, which has been a significant barrier for the large-scale preparation of novel zeolites that were synthesized using them.

Here, instead of using the large, bulky OSDAs, we are trying to fully utilize the roles of different framework T elements (T=Si, Ge, Al, and B) to synthesize novel zeolites. Many studies have shown that different framework T elements demonstrate the preferences in directing the formation of specific structure units under certain conditions as a result of different T-O bond lengths and T-O-T bond angles (Table below). The substitution of Si by B, Al, and Ge could form T-O-T with a smaller ∠T-O-T angle, allowing the construction of small building units such as *s*4*r* and *d*4*r*. Among B, Al, and Ge, B and Al show preferences to build the *s*4*r* unit, while Ge has advantages in forming the *d*4*r* unit.

The idea bond lengths and angles of different framework T elements[3-5]

T_1-O-T_2	r (T_1-O)/Å	r (T_1-O)/Å	∠T_1-O-T_2/°
Si-O-Si	1.61	1.61	145
Si-O-Al	1.61	1.70	138
Si-O-B	1.61	1.35	129
Si-O-Ge	1.61	1.74	138
Ge-O-Ge	1.74	1.74	133

Therefore, a synthesis system that combines multiple framework T elements ([Si,Ge,Al] and [Si,Ge,B]) and a simple, single OSDA was designed to synthesize zeolite materials. Such systems have received little attention before due to the very high opportunities to get the complex mixture products, which could be very difficult to analyze and purify[6-8]. The simple, single OSDAs are expected to mainly play the pore filling role during the crystallization, which would allow different framework T elements to have higher opportunities to form diverse structure building units and govern the formation of framework structures. The addition of Al or B into the synthesis system of germanosilicate zeolites could reduce the influence of Ge, increase the stability of the materials, create more active sites, and result in novel large or extra-large pore zeolites under simple, single OSDAs. The zeolite materials synthesized from our designed system would be promising for large-scale industrial production and application.

2. Chemicals and reagents

The chemicals and reagents used in the synthesis experiments include Ludox (SiO_2, HS-40, 40% Sigma-Aldrich), 4-dimethylaminopyridine (DMAP, 98wt%, TCI Shanghai), GeO_2 (99.0wt%, Sinopharm

Chemical Reagent Co. Ltd.), $Al(OH)_3$ (99.0wt%, Sinopharm Chemical Reagent Co. Ltd.), H_3BO_3 (99.0wt%, Sinopharm Chemical Reagent Co. Ltd.), HF (40wt% in water solution, Sinopharm Chemical Reagent Co. Ltd), and distilled water.

3. Synthesis of materials

In a typical synthesis procedure of the products prepared from [Si,Ge,Al] and [Si,Ge,B] systems, GeO_2 and DMAP (OSDA) were firstly added into the distilled water in a 23 ml Teflon liner, and the mixture was stirred at room temperature until GeO_2 and DMAP were dissolved. $Al(OH)_3$ or H_3BO_3 was then introduced under stirring. After $Al(OH)_3$ or H_3BO_3 was dissolved, Ludox was added. HF was introduced when the gel became homogeneous under stirring. In the end, the mixture was aged at room temperature for 2 hours under stirring. For the products synthesized from [Si,Ge] system, the step of introducing $Al(OH)_3$ or H_3BO_3 was omitted. The gels with compositions presented in Figure 1 were crystallized at 170 °C in 23 ml Teflon-lined stainless autoclaves under static condition for 10 days. For the synthesis of Product B, a two-step heating program (110 °C for 1 day and then 170 °C for 5 days) was applied for the crystallization. The gel composition is 1.0 SiO_2 : 0.2 GeO_2 : 0.048 Al_2O_3 : 0.6 OSDA : 0.6 HF : 10 H_2O (Si/Ge=5, (Si+Ge)/Al=12.5).

When the crystallization of gel was over, the autoclave was quenched with cold water. The solid product was recovered by centrifugation, washed with deionized water, and then dried at 110 °C for 12 hours. The organic species occluded in zeolite framework structures were removed by calcination at 600 °C for 5 h in the air atmosphere.

4. Characterization methods

All the electron diffraction data and translation electron microscope (TEM) images were collected on a JEOL JEM2100 LaB_6 TEM at 200 kV with a direct electron camera Timepix. For serial rotation electron diffraction (SerialRED), the typical setup uses the second smallest condenser lens aperture (which is around 10 microns in size when projected on the sample plane) globally. A partially condensed beam is used as a virtual "selected area" aperture for the 3D ED data collection of every single crystal. An exposure time of 0.5 s was used for diffraction pattern recording, and an image interval of 10 is used in checking the crystal position inside the virtual "selected area" aperture, which will automatically be changed to 2 when the algorithm detects the crystal is close to the edge of the aperture, to perform "robust" crystal tracking. Methods for automatic screening of suitable crystals, adjustment of eucentric height, and online crystal tracking have been discussed in our previous papers.[9,10] The samples were smashed into smaller particles before SerialRED experiments. For manual 3D ED data, it was collected with a similar procedure as that of SerialRED data. The data processing was conducted by REDp, XDS, and *edtools*[11].

Synchrotron powder X-ray diffraction (SPXRD) data were collected in a 0.5 mm capillary on the BL14B1 X-ray diffraction beamline at the Shanghai Synchrotron Radiation Facility in Shanghai, China using a wavelength of 0.68950 Å. The SPXRD patterns were collected in the 2θ range 2.500-38.000°

with 0.004° data binning. In-house powder X-ray diffraction (PXRD) patterns were recorded on a D8 Advance SS X-ray diffractometer using Cu Kα radiation, operating at 40 kV and 40 mA. Scanning electron microscopy (SEM) images were taken on a field emission XL30E scanning electron microscopy (FEI Company). Surface areas and pore volumes were obtained from N_2 adsorption/desorption isotherms using multipoint BET and t-plot methods. The experiments were performed on Micromeretic ASAP2020M physisorption apparatus at a liquid nitrogen temperature of -196 °C. The amounts of Si, Al, B, and Ge were quantified by inductively coupled plasma (ICP) on a Varian 725-ES instrument after dissolving the samples in HF solution. ^{29}Si, ^{27}Al, ^{13}C, and ^{19}F solid-state MAS NMR spectra were recorded on a Varian Model VNMRS-400WB spectrometer. ^{29}Si NMR spectra were acquired with a 7.5 mm T3HX probe at 79.43 MHz and a spinning rate of 3 kHz. ^{27}Al spectra were recorded at a frequency of 104.18 MHz, a spinning rate of 10.0 kHz, and a recycling delay of 4s. ^{13}C NMR spectra were recorded with a 7.5-mm T3HX probe at 100.54 MHz and a spinning rate of 5 kHz. ^{19}F solid-state NMR was recorded on a Bruker AVANCEIII 500WB spectrometer with a 2.5 mm probe at 376.5 MHz with a spinning rate of 30 kHz. The concentration of Lewis and Brønsted acid sites was determined after the adsorption of pyridine by FTIR spectroscopy on a Thermo Fisher Nicolet 380 spectrometer using the sample wafer. Temperature program desorption (TPD) using NH_3 was carried out in a TPD/TPR Altamira AMI-3300 equipment.

5. Catalytic reaction

5.1 Zeolite catalysts

The catalytic performances of **SFE** type aluminoborosilicate and Product B were tested in this work and compared with that of mordenite (**MOR**).

By using DAMP as OSDA, **SFE** type zeolite was synthesized in borogermanosilicate form in the beginning. Later, its borosilicate and aluminoborosilicate forms were also synthesized and have been reported by our group before.[12] Product B shows excellent thermal stability (Figure S15). ^{29}Si and ^{27}Al solid-state MAS NMR spectra reveal that almost all Si and Al atoms are four-coordinated in the framework structures after being calcined at 600 °C (Figure S19)[12]. N_2 adsorption and desorption isotherm demonstrate the microporous nature of this material (Figure S20). The BET surface area is 427 m^2g^{-1} with a micropore volume of 0.17 cm^3g^{-1} (Table S7). The NH_3-TPD curve and pyridine FT-IR spectra indicate that the calcined Product B possesses moderate acid intensity (Brønsted acid/Lewis acid=1.78, 400 °C, Figure S21 and S22). The details of **SFE** and **MOR** zeolite catalysts are presented in Figure S21, S22, and Table S7.

5.2 Reaction and testing

Disproportionation of the isopropylnaphthalene (IPN) is a complex reaction that produces numerous diisopropylnaphthalenes (DIPN) isomers, such as 1,3-DIPN, 1,7-DIPN, 2,6-DIPN (target product), and 2,7-DIPN. The 2,6-DIPN/2,7-DIPN ratio in the product is highly related to the pore architecture of zeolite catalysts, as revealed previously[13,14].

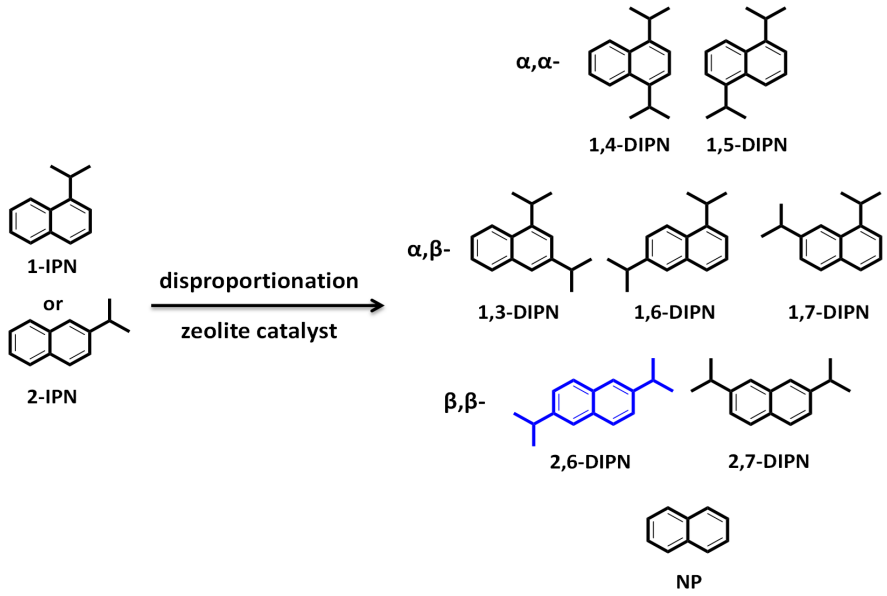

Possible products in the disproportionation of IPN. The increasing order of the critical size of DIPN molecules is 2,6-DIPN ⩽ 2,7-DIPN < 1,6-DIPN ⩽ 1,5-DIPN << 1,7-DIPN < 2,3-DIPN < 1,4-DIPN < 1,3-DIPN.[1] Disproportionation of the IPN is a complex reaction that produces numerous DIPN isomers, such as 1,3-DIPN, 1,7-DIPN, 2,6-DIPN (target product), and 2,7-DIPN.

Catalytic performances of Product B, **SFE**, and **MOR** were tested in the disproportionation of isopropylnaphthalene (97.6 wt% (65.1 wt% 2-PIN in IPN), purchased from China Medicine Group). H-form Product B catalyst was obtained directly via calcination of as-made products in the air at 600 °C for 5 h. Disproportionation reactions were conducted in a 100 ml stainless steel autoclave with magnetic agitation under reaction conditions as follows: 35 g INP : 1.5 g catalyst, autogenous pressure, 250 °C, and reaction time of 6 h. After the reaction was finished, the autoclave was cooled down to room temperature by water, and the catalysts were filtrated. The reaction products were analyzed by an Agilent 7890A Gas Chromatograph equipped with an Agilent 19091N-236 HP-INNOWax capillary column (60 m × 250 μm × 0.5 μm) by using an FID detector.

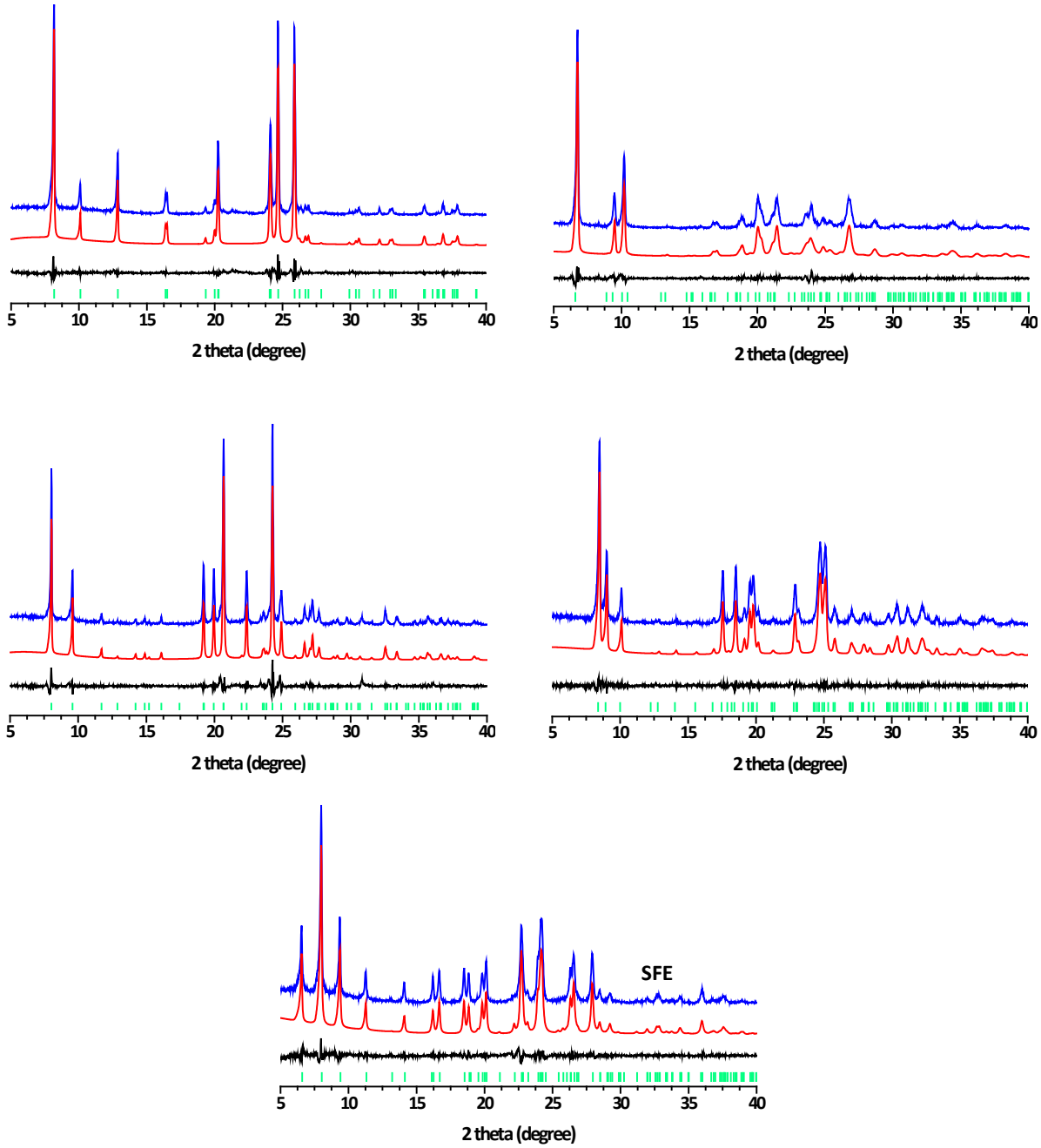

Figure S1 Pawley fit of the PXRD patterns (Cu Kα) of pure phase zeolites obtained in exploring our designed synthesis system. Observed (blue line), calculated (red line), as well as difference (black line) profiles are presented. The green tick marks under the patterns are the positions of the Bragg reflections. The phase information of the pure phase zeolites synthesized in our system was well identified by PXRD.

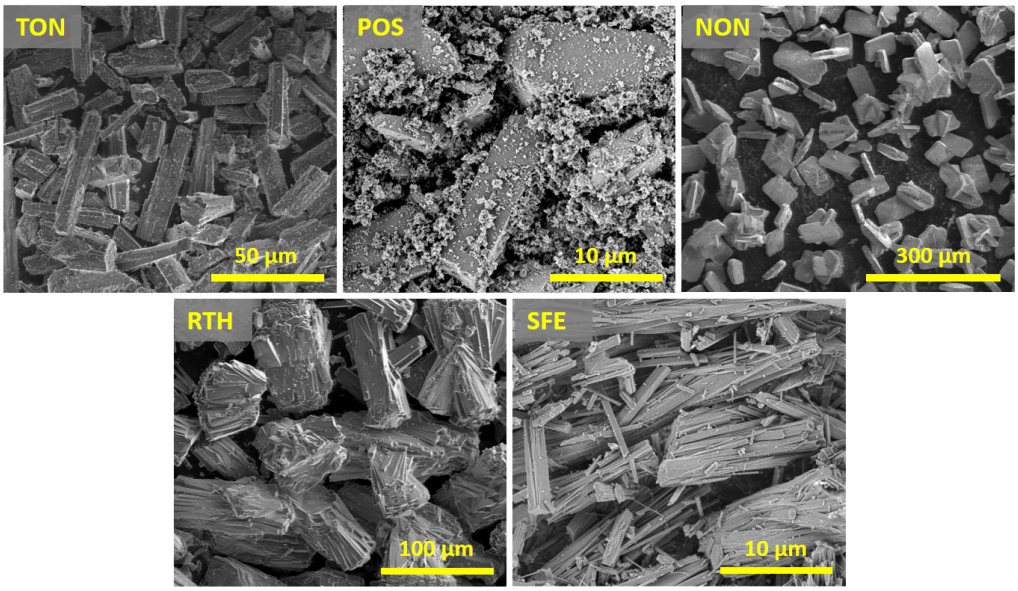

Figure S2 SEM images of the pure phase zeolites (**POS** contains some amorphous) obtained in exploring our designed synthesis system under the utilization of a simple, small amine (DAMP) as OSDA. **TON**, **POS**, **RTH**, and **SFE** all show needle-like morphologies.

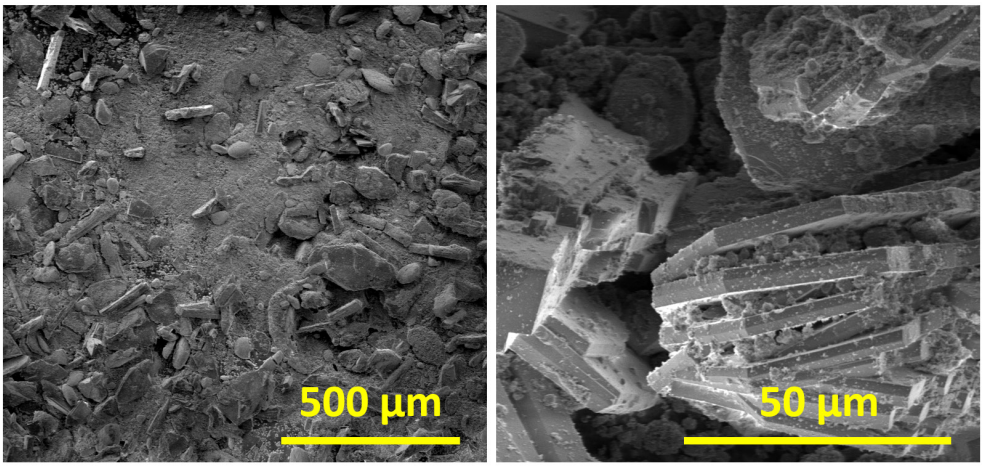

Figure S3 SEM images (with different magnifications) of Product A. Crystals with the needle- and plate-like morphologies could be observed.

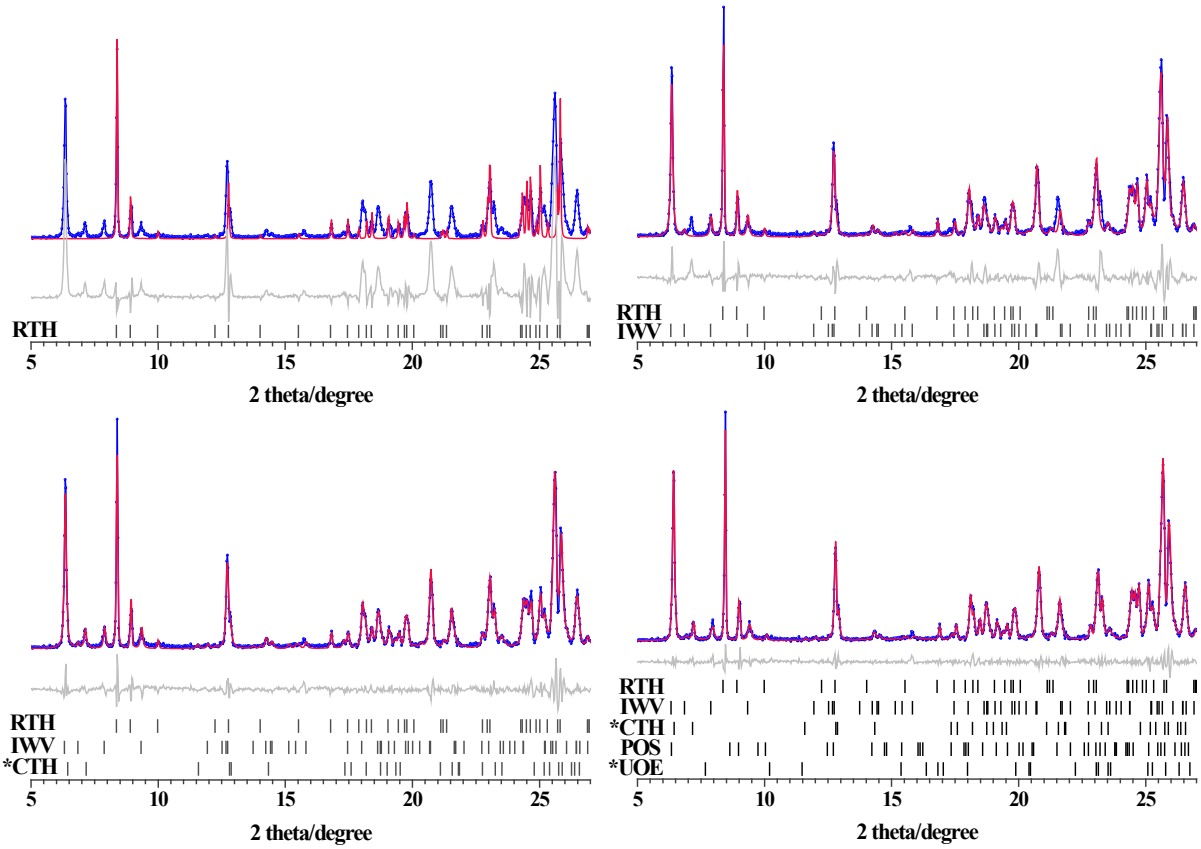

Figure S4 Pawley fit of the PXRD pattern (Cu Kα) of Product A with different phases: a) **RTH**, b) **RTH** and **IWV**, c) **RTH**, **IWV**, and ***CTH**, and d) **RTH**, **IWV**, ***CTH**, **POS**, and ***UOE**. Observed (blue dots), calculated (red line), as well as difference (grey line) profiles are presented. The tick marks are the positions of the Bragg reflections belonging to each phase. The unindexed reflections were highlighted with the black stars. Without the aids of 3D ED techniques, only **RTH** could be identified based on the PXRD data. The phase (***CTH**) ignored by manual 3D ED and the phases (**POS** and ***UOE**) impossible to be detected by PXRD are all elucidated reliably using SerialRED.

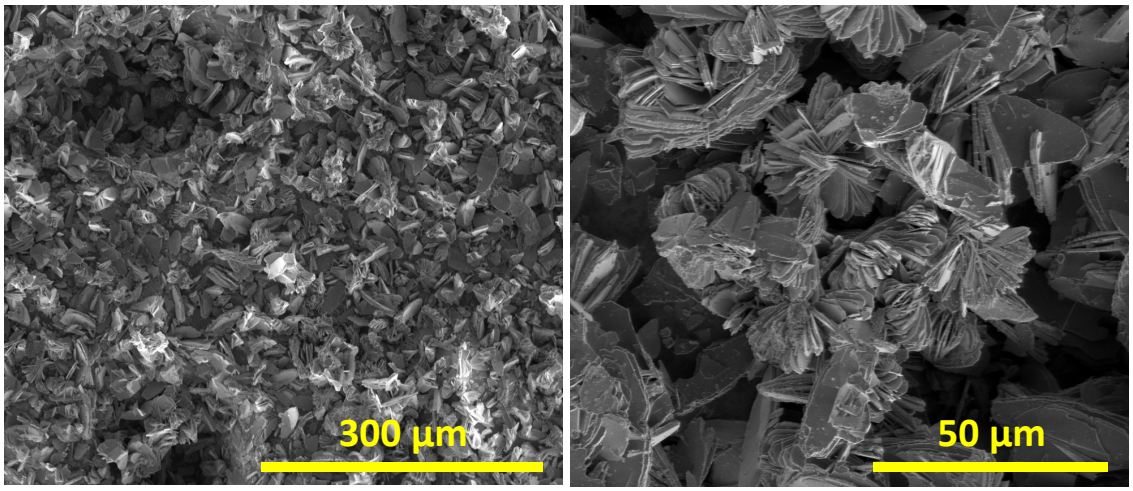

Figure S5 SEM images (with different magnifications) of Product B. Only the high-quality crystals with unified plate-like morphology were observed, which indicates Product B might be a pure phase.

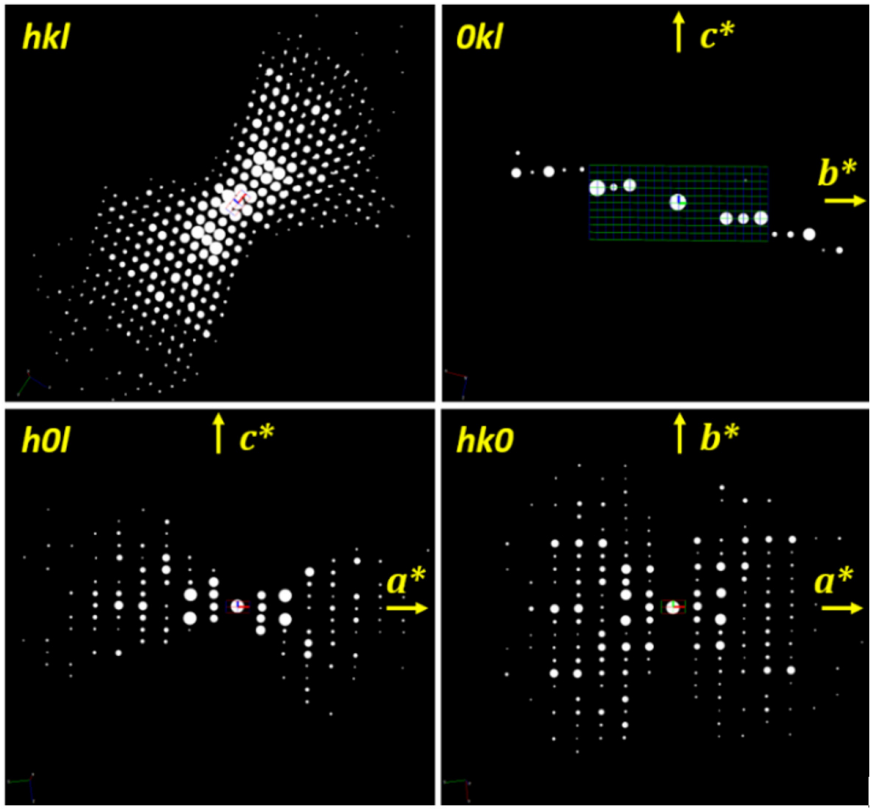

Figure S6 Reciprocal lattice of one plate-like crystal in Product B reconstructed from the manually collected 3D ED data. The reflection conditions deduced from the 3D reciprocal lattice and the three 2D slices are *hkl*: *h*+*k*=2n, *h*+*l*=2n, *k*+*l*=2n, 0*kl*: *k*=2n, *l*=2n, *h*0*l*: *h*=2n, *l*=2n, *hk*0: *h*=2n, *k*=2n, *h*00: *h*=2n, 0*k*0: *k*=2n, 00*l*: *l*=2n. An orthorhombic unit cell (a= 14.34Å, b= 26.11Å, c=28.81Å) with possible symmetries of *Fmmm*, *Fmm2*, and *F222* was elucidated, which is in good agreement with the unit cell of **IWV** zeolite. The resolved structure model further confirmed that Product B contains a zeolite with an **IWV** type of framework.

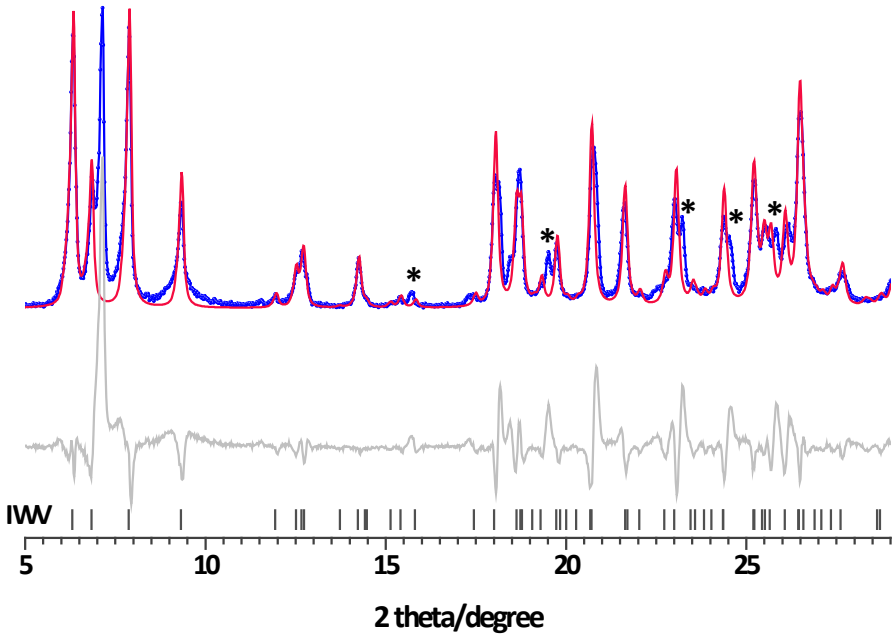

Figure S7 Pawley fit of the PXRD pattern (Cu Kα) of Product B with phase **IWV**. Observed (blue dots), calculated (red line), as well as difference (grey line) profiles are presented. The difference profile shows that considerable strong reflections were not indexed (highlighted with black stars). This indicates that Product B may contain another phase, and PXRD and manual 3D ED failed to identify it.

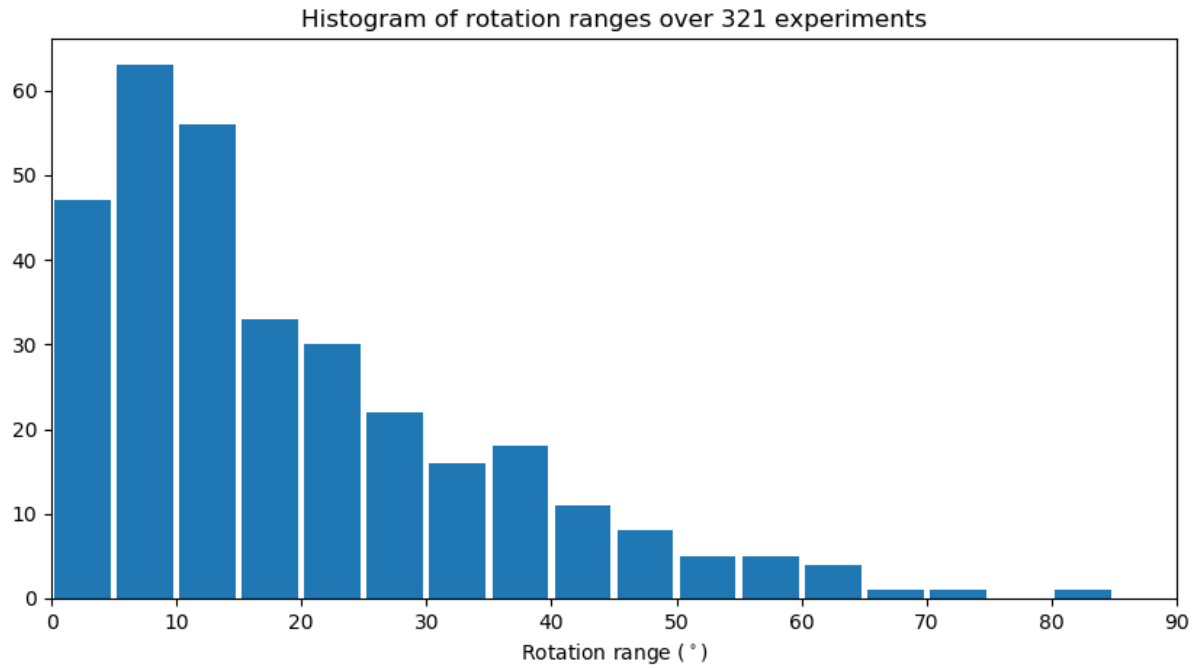

Figure S8. Rotation range histogram for the SerialRED experiment on Product A. 321 data sets were collected within a 6 hours' runtime.

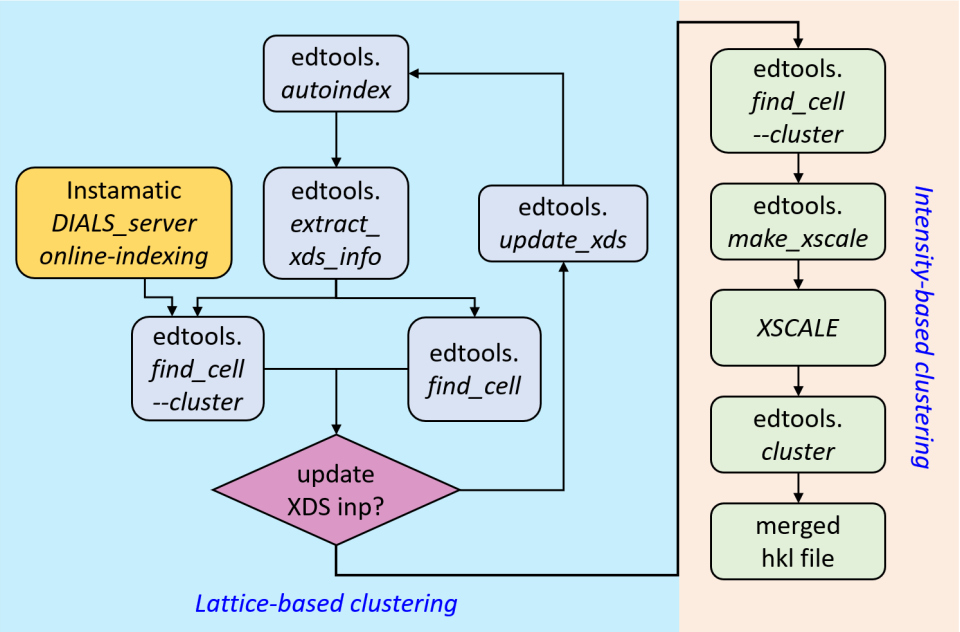

Figure S9 Flowchart of the analysis of SerialRED data by *edtools*. The hierarchical clustering analysis (HCA) is performed in two steps: lattice-based clustering and intensity-based clustering. For datasets with sufficiently different unit cell parameters (identified by *DIALS* or *XDS*), lattice-based clustering tells them apart by applying the modified Euclidean distance (Eq. S1) as the metric. For datasets with similar or the same unit cell parameters, they can be separated effectively using a second step intensity-based clustering, taking the Pearson correlation coefficient between symmetry-related reflections in two datasets (calculated by *XSCALE*) as the distance metric[11]. Clustered datasets after the two steps will be automatically merged using *XSCALE*, and the obtained intensity files can be directly used for structure determination and refinement.

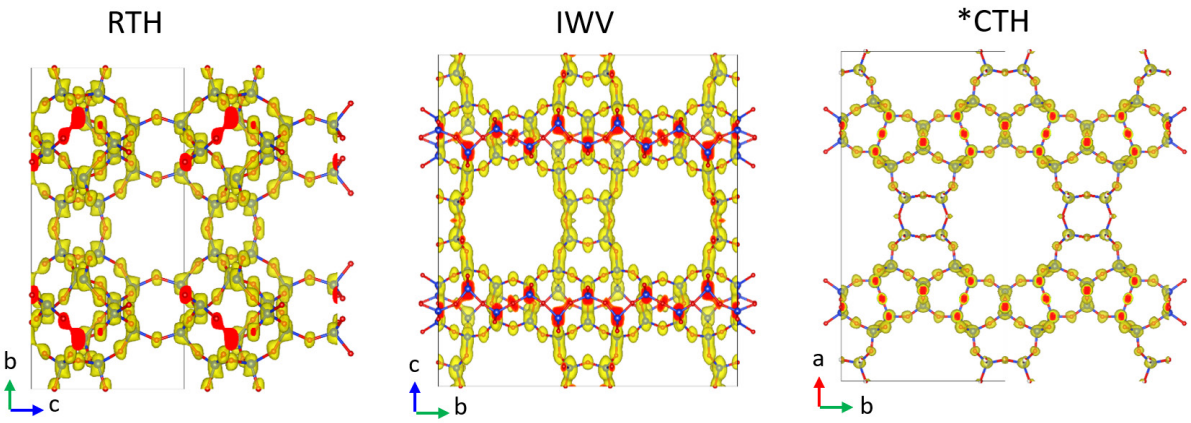

Figure S10 Framework structures and corresponding observed electron density maps of the major phases **RTH**, **IWV**, and ***CTH** resolved by the merged SerialRED data. This demonstrates that SerialRED is not only a powerful method in phase analysis but also structure determination. All the atoms in these three framework structures (***CTH** has a complex framework structure that contains disorder) could be directly resolved based on the merged SerialRED data.

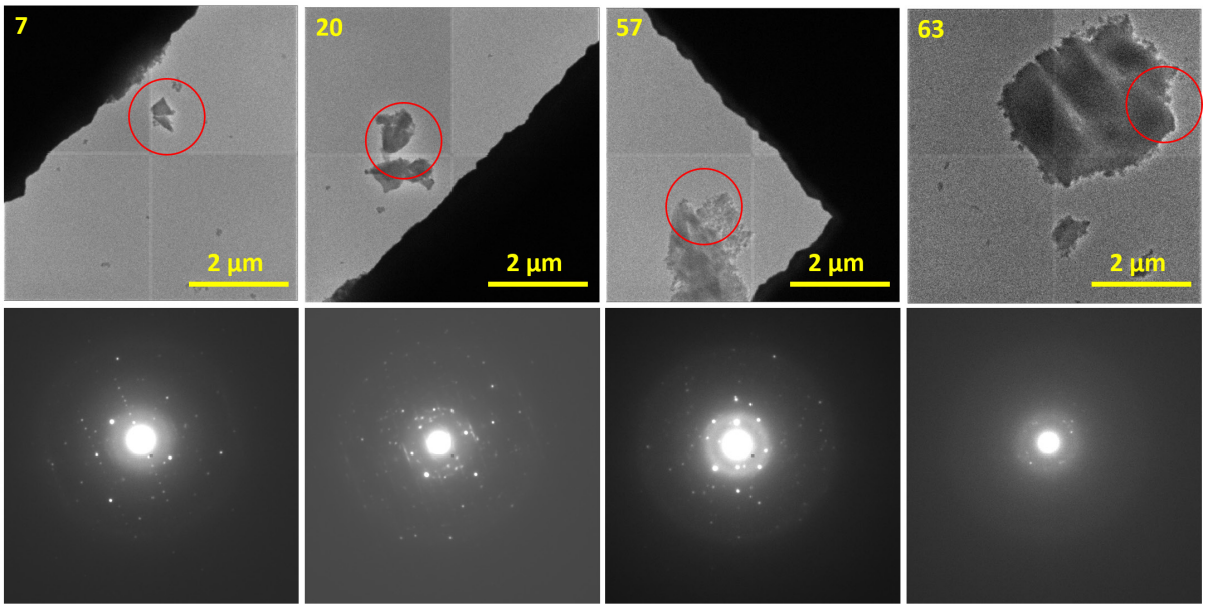

Figure S11 TEM images (up) and corresponding diffraction patterns (down) of selected crystals with their unit cells unclassified in Figure 3 and Table S3. The numbers in yellow at the upper left corner of each image are the dataset indexes in Figure 3 and Table S3. The unclassified unit cells majorly belong to datasets of multiple lattices (7, 20, 57) or bad quality (63), resulting in unit cell parameters with large deviations or being completely incorrect.

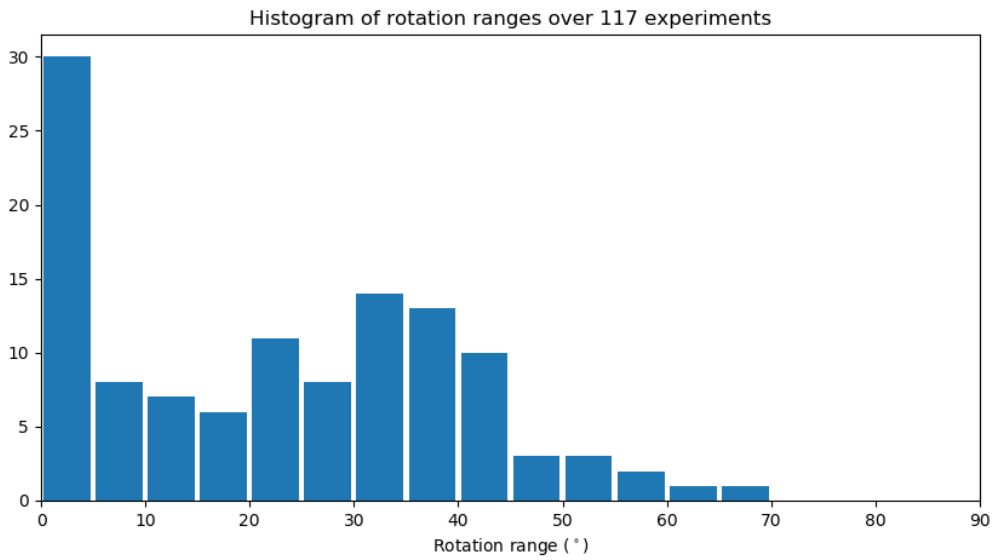

Figure S12 Rotation range histogram for the SerialRED experiment on Product B. 117 data sets were collected within a 4 hours' runtime.

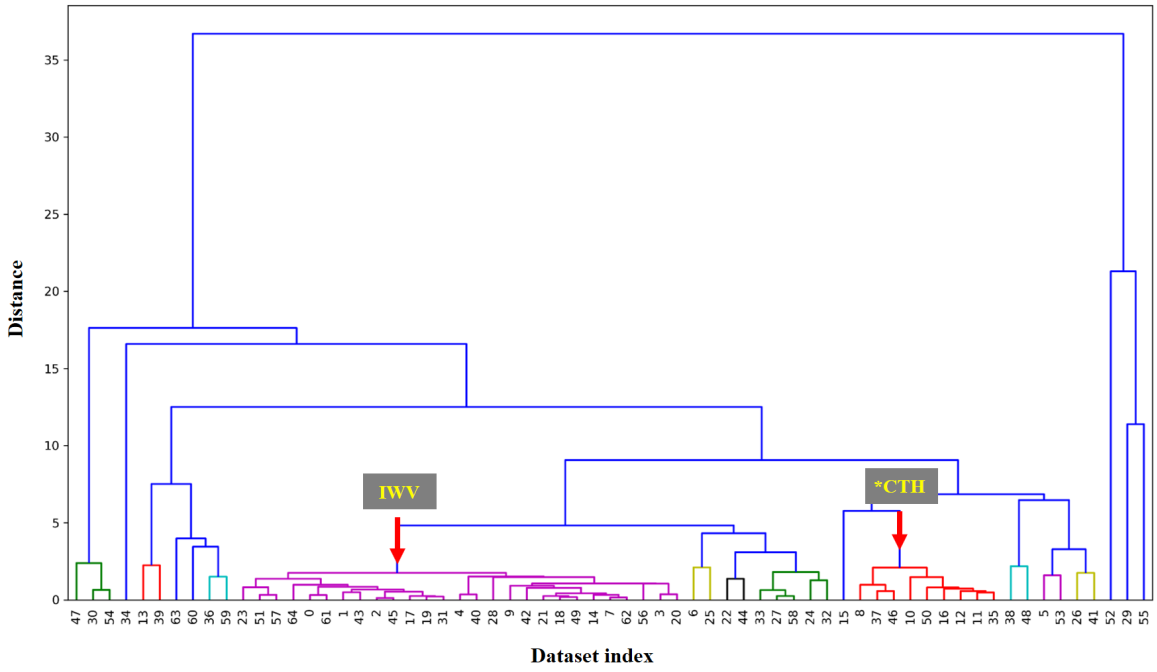

Figure S13 HCA on preliminary indexing results parsed from XPARM.XDS files from *XDS* processing. In total, 117 datasets were collected during a 4-hour' automated run of SerialRED. Among them, 89 datasets returned unit cell determination results, out of which 65 were with rotation ranges larger than 20˚. Two zeolite phases including **IWV** and ***CTH** were revealed by HCA with a distance threshold set at 3.0. The unclassified data sets can be attributed to the multi-lattices and/or bad data quality, which will result in incorrect unit cell parameters. In Product B, the **IWV** and ***CTH** have the same plate-like crystals. They can be aggregated together easily, resulting in many SerialRED data sets from multi-crystals. The unit cell parameters of all data sets are shown in Table S4. Here we opted to use preliminary unit cell determination results from XPARM.XDS instead of the *DIALS* server because the clustering result seemed to be clearer with XPARM.XDS. For product A, the clustering result turned out to be quite similar to either *DIALS* results or XPARM.XDS results, and we ended up using the results from *DIALS*.

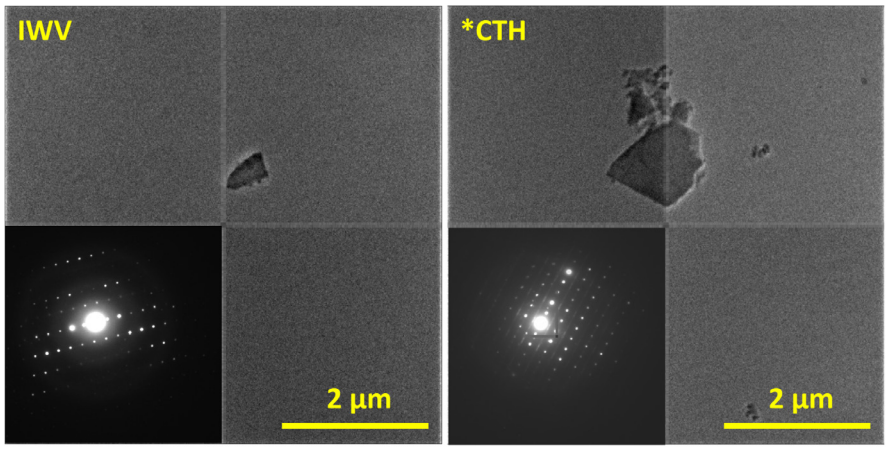

Figure S14 The typical morphologies and corresponding electron diffraction patterns (bottom left) of the smashed crystals of **IWV** and ***CTH**.

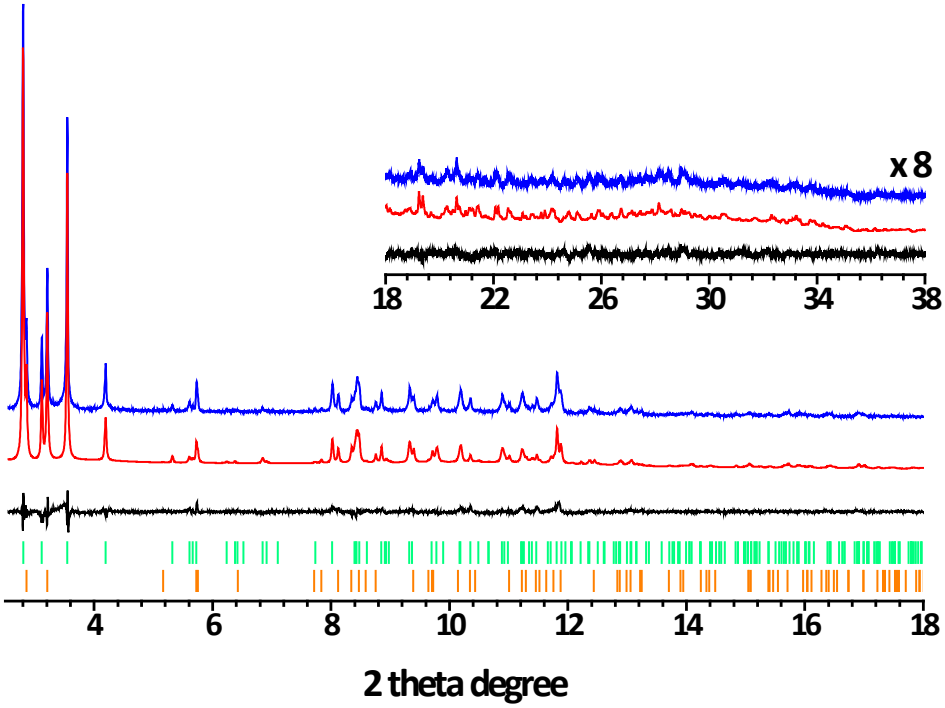

Figure S15 Rietveld refinement of Product B (calcined) against the SPXRD data (wavelength: 0.6895 Å). Observed (blue line), calculated (red line), as well as difference (black line) profiles are presented. The profiles in the inset have been magnified by eight times to show more details. The green and pink tick marks under the patterns are the positions of the Bragg reflections belonging to **IWV** and ***CTH**, respectively. The refined phase composition is 67% **IWV**: 33% ***CTH**. Due to the relatively low phase content and peak overlapping, it is almost impossible to identify the phase ***CTH** by PXRD.

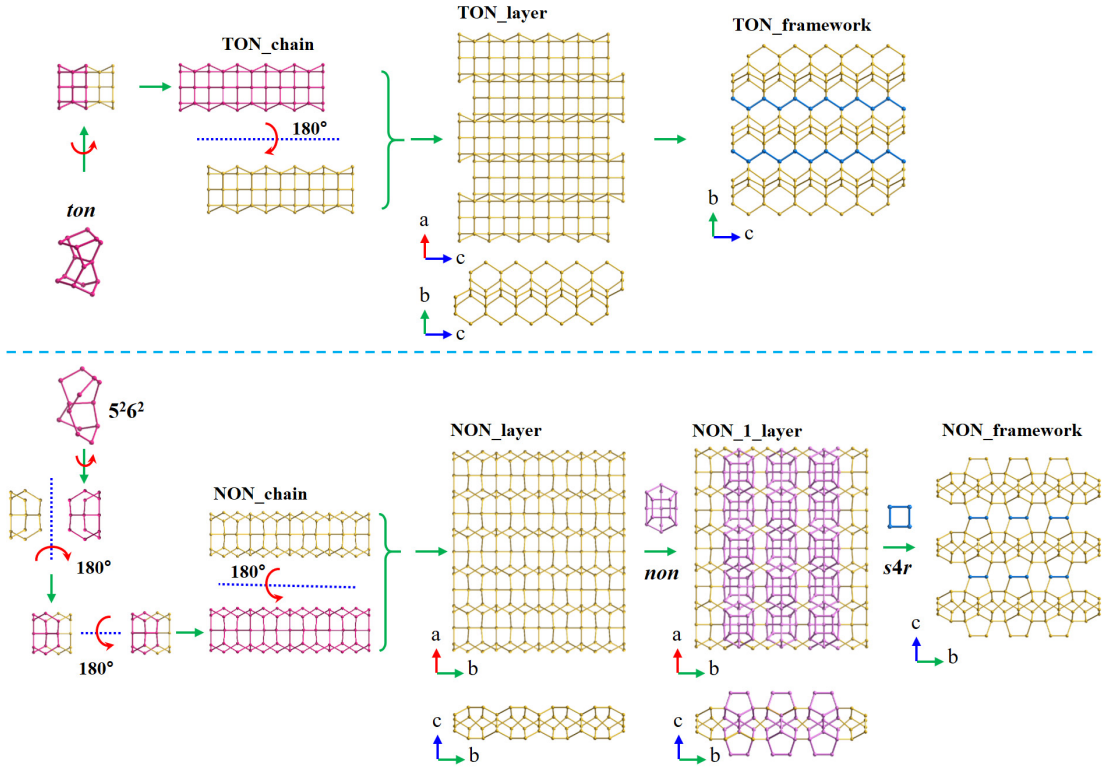

Figure S16 Structural relationship between **TON** and **NON**. The frameworks of them contain very similar layers (*TON_layer* and *NON_layer*) that are constructed from very similar building units (*ton*, 5^26^2). **TON** framework can be directly formed from the *TON_layers*, while **NON** framework can be built by the *NON_1_layers*, which were constructed after embedding *non* units on the *NON_layers*. The formation of **NON** (Si/Ge=15, (Si+Ge)/T^{III}=30~100) type framework structure was realized by introducing a small amount of Al or B into the synthesis system of **TON** (Si/Ge=15, (Si+Ge)/T^{III}=∞), which indicates Al or B triggers the formation of *non* building units. While Si and a small amount of Ge are responsible for forming the very similar *TON*- and *NON-layer* in **TON** and **NON** frameworks, respectively.

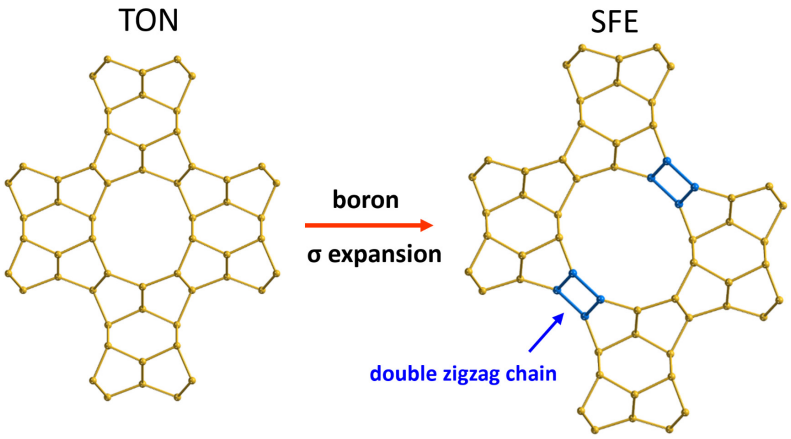

Figure S17 Structure relationship between **TON** and **SFE**. **SFE** type framework structure could be constructed from that of **TON** through σ expansion. The σ expansion and formation of **SFE** (Si/Ge=15, (Si+Ge)/B=5-25) could be achieved by introducing a significant amount of B into the synthesis system of **TON** (Si/Ge=15, (Si+Ge)/B=∞), which shows B has the advantage in directing the formation of the small *s*4*r* units and building the double zigzag chains.

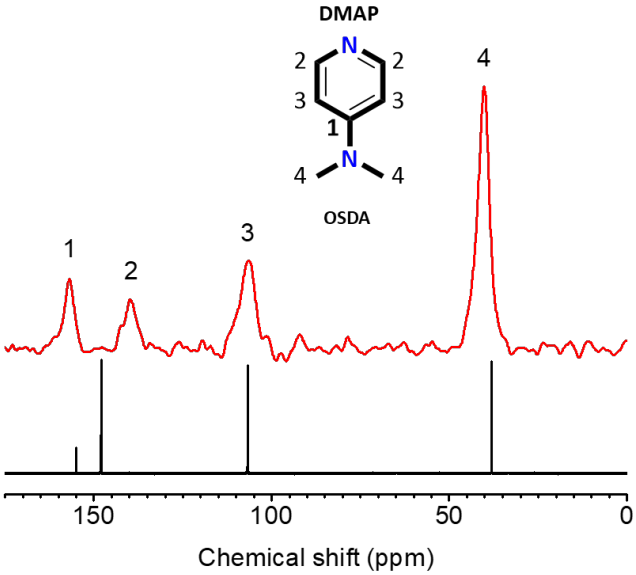

Figure S18 ^{13}C liquid NMR spectrum of DMAP and ^{13}C solid-state MAS NMR spectrum of as-made Product B. DMAP molecules remain intact within the framework structures.

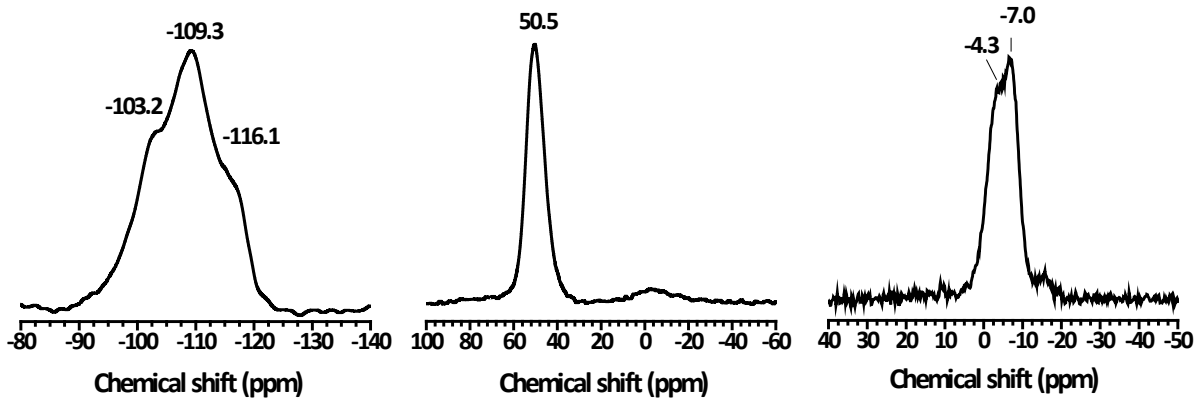

Figure S19 ^{29}Si, ^{27}Al, and ^{19}F solid-state NMR spectra of Product B. The spectra reveal that almost all Si and Al atoms are four-coordinated in the framework structures. In addition, ^{19}F NMR spectrum indicates considerable Ge atoms are located in *d*4*r* units.

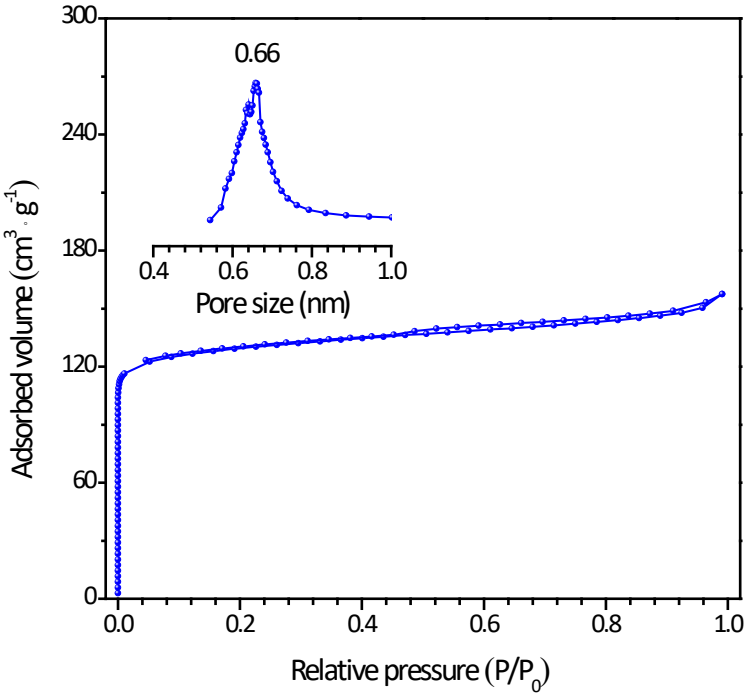

Figure S20 N_2 adsorption/desorption isotherms and pore size distribution of the calcined Product B.

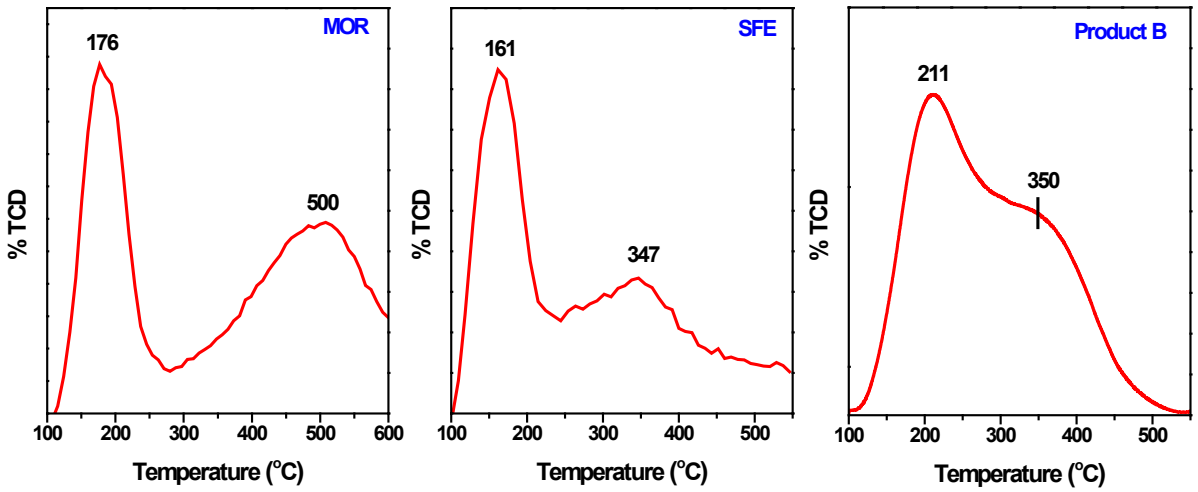

Figure S21 NH_3-TPD curves of **MOR**, **SFE**, and Product B. The intensity and concentration of the strong acid of **MOR** (Si/Al=18) are higher than those of **SFE** (Si/B=84, Si/Al=57) and Product B (Si/Ge=6, Si/Al=17). Conversely, **SFE** and Product B possess moderate acid intensity.

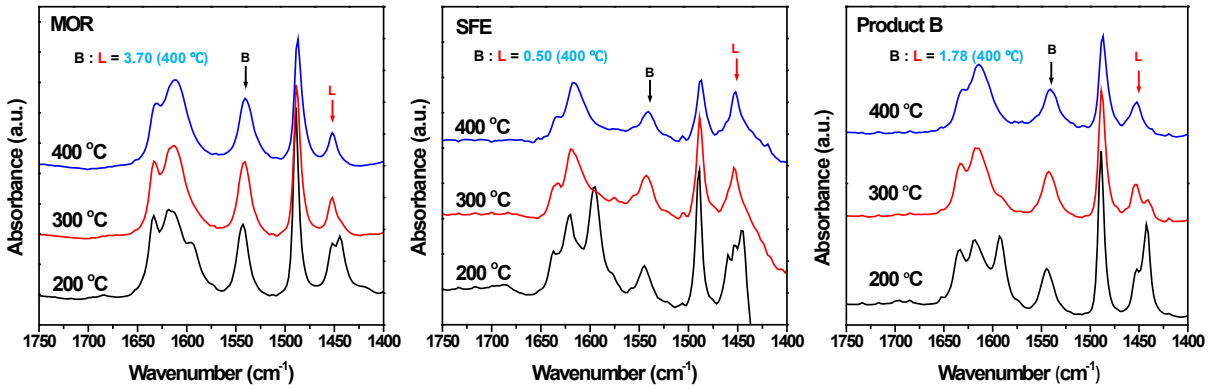

Figure S22 FT-IR spectra of **MOR**, **SFE**, and Product B after adsorbing pyridine followed by desorption at different temperatures. The strong acid in **MOR** and **SFE** is dominated by Brönsted acid (B : L=3.70, 400 °C) and Lewis acid (B : L=0.5), respectively. While in Product B, the concentration of Brönsted acid is higher than that of Lewis acid but with moderate ratios (B : L=1.78) compared with those of **MOR** and **SFE**.

Table S1 SerialRED results of Product A from first-step lattice-based clustering (The index of data sets corresponds to the index shown in Figure 3).

Group index	Dataset index: Determined unit cell in standardized P1 setting	Rotation range	Phase
1	0 : [13.96 14.33 14.68 75.51 68.44 62.38]	20.24	**IWV**
	3 : [12.86 13.98 15.51 78.34 67.46 65.18]	59.60	
	4 : [13.13 13.91 13.96 77.10 64.10 62.92]	40.09	
	8 : [12.85 14.14 15.32 78.52 66.70 65.39]	36.15	
	9 : [12.86 13.97 14.18 79.44 67.72 64.80]	44.09	
	17 : [13.77 14.31 14.61 76.67 63.22 62.72]	66.93	
	19 : [13.95 14.01 15.88 79.01 67.37 61.07]	64.25	
	29 : [14.74 14.92 17.05 82.80 69.10 62.17]	21.85	
	32 : [13.38 14.26 14.50 77.96 66.13 63.73]	37.07	
	37 : [13.81 14.17 14.61 75.10 66.50 63.84]	35.15	
	39 : [13.88 14.41 15.74 79.93 66.14 62.00]	25.40	
	42 : [13.53 14.14 14.24 78.45 63.67 62.41]	27.41	
	46 : [12.71 13.00 14.18 84.43 67.90 64.16]	31.72	
	47 : [13.76 14.88 16.01 80.19 65.75 66.07]	59.50	
	59 : [13.70 14.29 14.79 78.61 62.57 63.15]	44.50	
	69 : [14.14 14.63 15.88 102.64 104.82 116.34][a]	25.92	
	70 : [13.20 13.82 14.13 76.28 63.05 63.31]	38.13	
	71 : [14.08 14.42 16.48 71.53 65.21 62.15]	22.46	
	72 : [14.00 13.56 16.05 78.31 66.55 61.85]	30.70	
	73 : [14.87 14.45 15.71 75.84 62.84 63.19]	31.06	
2	1 : [9.90 10.86 11.07 75.59 74.24 76.42]	22.76	**RTH**
	2 : [9.52 10.26 10.99 85.42 67.36 81.10]	22.57	
	6 : [9.81 10.11 11.53 87.83 70.59 79.88]	26.10	
	11 : [9.71 10.44 12.04 83.33 69.63 83.99]	38.84	
	16 : [9.72 10.24 10.79 101.55 90.20 90.50]	35.40	
	18 : [10.08 10.60 11.66 68.3 83.33 85.40]	40.15	
	21 : [9.24 9.46 11.11 66.93 86.98 83.08]	49.80	
	24 : [10.26 10.45 11.44 82.80 64.26 79.09]	28.27	
	25 : [9.20 9.28 10.78 83.00 65.63 83.70]	24.50	
	31 : [9.30 9.50 10.82 66.25 82.97 83.90]	26.91	
	38 : [9.44 9.87 10.95 113.64 90.51 97.71]	60.20	
	44 : [10.16 10.39 12.24 95.52 113.75 96.75]	22.06	
	49 : [9.58 10.23 12.34 88.05 70.19 84.12]	30.80	
	53 : [9.29 9.56 10.15 89.54 65.42 86.06]	31.76	
	54 : [9.67 9.67 11.13 68.90 84.10 82.80]	53.23	
	55 : [10.32 10.82 11.73 79.84 65.49 80.99]	22.59	
	58 : [9.43 9.53 11.07 92.39 112.91 94.90]	48.99	
3	5 : [4.65 12.82 14.79 64.95 88.74 87.05]	37.23	***CTH**
	13 : [4.94 13.23 14.87 64.39 85.76 88.32]	35.50	
	14 : [5.22 15.07 15.62 110.73 94.96 99.14][a]	27.21	
	23 : [4.82 14.06 15.10 64.41 87.47 89.49]	27.57	
	26 : [5.21 13.63 15.49 115.93 98.06 92.09][a]	31.25	
	27 : [5.67 13.91 15.71 64.08 89.34 87.58]	35.29	
	28 : [4.96 14.69 15.57 113.37 91.01 91.67][a]	44.09	
	30 : [5.25 14.36 15.00 66.33 87.6 84.59]	33.68	
	34 : [5.40 13.50 16.05 108.90 94.10 93.10][a]	25.00	
	35 : [5.01 13.38 14.08 64.35 85.18 86.96]	44.29	
	36 : [4.88 12.70 14.37 68.50 86.34 89.20]	49.49	
	45 : [5.52 15.08 16.23 110.81 92.17 93.60][a]	25.34	
	48 : [5.39 13.95 15.22 63.08 88.49 89.70]	26.86	
	50 : [5.13 14.71 15.72 62.13 88.50 83.10]	22.37	
	51 : [5.22 13.42 15.53 112.63 91.57 93.47][a]	32.63	
	52 : [5.17 13.51 15.56 70.00 89.41 88.98][a]	45.46	
	56 : [5.29 14.34 16.05 67.24 89.24 89.25]	35.10	
	62 : [5.46 14.46 16.05 70.34 88.89 88.68]	30.90	

	64 : [5.07 14.47 14.65 118.60 91.50 90.20]	22.42	
	67 : [5.01 13.46 14.93 64.73 86.06 86.15]	54.04	
	75 : [5.22 13.64 14.27 116.37 90.93 90.29]	22.72	
	76 : [5.28 13.98 16.47 69.38 86.59 87.62]	26.12	
4	7 : [4.92 10.75 11.03 79.79 77.78 80.18]	27.72	Unclassified
5	10 : [4.83 4.94 5.15 92.29 92.24 115.58]	22.73	SiO_2/GeO_2
	74 : [4.18 4.44 5.67 90.50 110.83 111.36]	35.35	
6	12 : [5.16 11.94 12.72 83.00 81.81 77.84]	45.30	***UOE**
	15 : [5.18 12.17 13.97 79.60 82.50 79.50]	39.96	
7	20 : [5.26 8.29 14.40 77.10 84.5 84.10]	57.84	Unclassified
	65 : [5.27 8.00 12.54 95.20 102.10 94.10]	80.17	
8	22 : [4.96 5.37 6.80 81.10 89.40 67.80]	35.60	SiO_2/GeO_2
	41 : [5.27 6.05 7.10 90.92 111.02 106.80]	31.05	
9	33 : [9.95 13.80 14.82 65.44 88.19 89.47]	26.75	Unclassified
	57 : [9.52 13.79 15.65 65.85 88.64 85.72]	23.73	Unclassified
10	40 : [10.95 18.76 19.37 89.23 87.17 87.4]	27.52	**POS**
11	43 : [4.85 15.87 15.89 117.00 92.10 93.80]	43.94	Unclassified
12	60 : [6.92 7.64 8.49 66.60 69.40 80.80]	34.96	Unclassified
13	61 : [4.75 4.83 9.90 89.81 88.29 61.97]	48.90	Unclassified
14	63 : [4.78 8.25 9.60 69.90 85.98 88.70]	37.93	Unclassified
	68 : [5.19 7.49 8.32 94.86 107.50 96.70]	63.85	
15	66 : [3.18 9.73 11.27 65.62 87.45 87.35]	49.55	Unclassified

[a] unit cell with supplementary angles

As to make unit cell dimensions from data sets with different data quality comparable, the determined unit cell from *DIALS* is always extracted in $P1$ setting. This is to eliminate the unit cell difference that comes merely from the transformation with lattice symmetry. The distance metric used in the clustering is defined as (Eq. S1):

$$d_{i,j} = \sqrt{\Delta a_{i,j}^2 + \Delta b_{i,j}^2 + \Delta c_{i,j}^2 + \Delta(\sin\alpha)_{i,j}^2 + \Delta(\sin\beta)_{i,j}^2 + \Delta(\sin\gamma)_{i,j}^2}$$

where the angle terms are sine converted in order to flatten the ambiguity from indexing (*e.g.* an angle can be either 60˚ or 120˚ regarding the same unit cell). The distance metric in Eq. S1 is derived from the metric LCV (linear cell variation)[15]. Here, the defined distance metric follows a direct intuition to be able to group unit cells of the same phases purely based on the magnitudes of the 6 numbers of unit cell parameters; not much optimization effort has been made to the weighting scheme for the length numbers and angle numbers, which we believe could potentially further improve the clustering results.

The deviations of unit cell parameters are a little bit big, especially the angles. This can be mainly ascribed to the moving of crystal, the shifting of the direct central beam, and the relatively low rotation range. The unclassified unit cells majorly belong to data sets of multiple lattices or bad data quality, resulting in unit cell parameters with large deviations or are wrong.

Table S2 Primitive unit cells and the corresponding unit cells with the highest symmetry of different zeolites

Phase	Primitive unit cell parameters						Space group
RTH	*a*=10.3Å	*b*=10.5 Å	*c*=11.6 Å	α=89.0°	*β*=65.7°	γ=85.0°	*P1*
IWV	*a*=14.4 Å	*b*=14.5 Å	*c*=15.5 Å	α=77.8°	*β*=63.0°	γ=62.0°	*P1*
***CTH**	*a*=5.0 Å	*b*=13.8 Å	*c*=15.0 Å	α=65.0°	*β*=90.0°	γ=90.0°	*P1*
POS	*a*=11.9 Å	*b*=19.6 Å	*c*=19.6 Å	α=90.0°	*β*=90.0°	γ=90.0°	*P1*
***UOE**	*a*= 5.3 Å	*b*=11.8 Å	*c*=12.0 Å	α=80.0°	*β*=79.0°	γ=79.0°	*P1*
Phase	Unit cells with highest symmetry						Space group
RTH	*a*=10.3 Å	*b*=21.2 Å	*c*=10.5 Å	α=90.0°	*β*=95.0°	γ=90.0°	(*C2/m*)
IWV	*a*=14.4 Å	*b*=25.6 Å	*c*=27.6 Å	α=90.0°	*β*=90.0°	γ=90.0°	(*Fmmm*)
***CTH**	*a*=5.0 Å	*b*=27.2 Å	*c*=13.8 Å	α=90.0°	*β*=90.0°	γ=90.0°	(*Cmmm*)
POS	*a*=19.6 Å	*b*=19.6 Å	*c*=11.9 Å	α=90.0°	*β*=90.0°	γ=90.0°	($P4_2/mnm$)
***UOE**	*a*=5.3 Å	*b*=15.3 Å	*c*=17.7 Å	α=90.0°	*β*=90.0°	γ=90.0°	(*Immm*)

Table S3. Crystallographic information of the three major phases that were resolved using SerialRED data in Product A.

Phase	**RTH**	**IWV**	***CTH**
Unit cell (Å)	9.68, 20.83, 10.00, β=95.4˚	27.83, 26.08, 13.94	13.69, 27.50, 5.04
Space group	$C2/m$	$Fmmm$	$Cmm2$
Resolution (Å)	1.0	0.8	0.8
Completeness (%)	52.0 (5 data sets)	97.6 (8 data sets)	79.9 (5 data sets)
$R_{int}/R_1/wR_2$	0.1238/0.2736/0.6111	0.2908/0.3165/0.6678	0.1375/0.2165/0.5162
No. of reflections (observed)	624 (397)	2549 (1202)	1565 (1135)
No. of parameters (restraints)	113 (108)	153 (218)	69 (25)

Table S4 SerialRED results of Product B from first-step lattice-based clustering (single dataset clusters are omitted).

Group index	Dataset index: Determined unit cell in standardized P1 setting	Rotation range	Phase
1	0 : [13.51 13.96 15.53 66.85 82.20 68.18]	37.80	**IWV**
	1 : [13.51 14.41 14.79 81.25 66.51 66.49]	22.93	
	2 : [13.99 13.99 14.89 76.67 68.88 62.50]	43.76	
	3 : [13.76 14.99 15.56 80.70 63.03 66.01]	39.51	
	4 : [15.03 15.50 16.50 69.78 61.75 78.47]	21.47	
	7 : [13.95 14.55 16.38 80.73 70.94 62.66]	29.27	
	9 : [13.77 13.79 16.45 81.07 64.99 63.98]	35.97	
	14 : [14.19 14.30 16.58 80.73 68.22 62.64]	29.31	
	17 : [13.95 14.67 15.01 78.80 65.03 66.41]	34.20	
	18 : [14.25 14.63 16.28 67.77 77.93 66.24]	21.09	
	19 : [13.94 14.45 15.16 81.28 70.52 62.11]	51.98	
	20 : [13.65 14.76 15.78 61.56 78.18 65.66]	39.41	
	21 : [14.31 14.39 16.17 76.51 65.97 65.74]	30.38	
	23 : [15.01 15.17 15.53 79.83 77.61 63.55]	33.90	
	28 : [13.79 14.90 17.60 81.22 67.33 63.35]	34.16	
	31 : [13.91 14.44 14.96 73.89 67.53 62.84]	30.77	
	40 : [15.27 15.38 16.68 81.94 71.91 60.21]	41.48	
	42 : [14.56 14.66 16.95 76.01 66.74 60.97]	47.65	
	43 : [13.57 14.08 14.41 81.33 68.94 61.98]	39.61	
	45 : [14.02 14.05 14.85 62.52 74.19 62.44]	50.67	
	49 : [14.32 14.62 16.12 78.48 68.78 66.26]	21.32	
	51 : [14.63 14.73 14.82 63.91 74.74 60.53]	31.07	
	56 : [14.10 15.44 16.43 79.29 68.67 76.94]	44.21	
	57 : [14.58 14.93 15.03 80.57 61.18 69.27]	58.50	
	61 : [13.78 13.84 15.41 105.25 100.76 117.26]	38.14	
	62 : [14.07 14.48 16.43 68.05 77.96 62.02]	34.06	
	64 : [13.09 13.73 14.87 84.39 65.30 66.94]	36.94	
2	5 : [11.09 13.21 14.34 93.21 93.86 110.60]	26.89	Unclassified
	53 : [10.79 12.68 12.89 48.11 86.65 87.99]	51.78	
3	6 : [10.74 15.29 19.96 105.53 85.02 107.55]	42.33	Unclassified
	25 : [9.94 13.53 20.78 50.55 79.24 82.82]	35.31	
4	8 : [5.08 15.23 17.79 70.44 84.59 89.18]	41.83	***CTH**
	10 : [4.95 13.80 16.77 101.83 86.54 88.43]	26.28	
	11 : [5.27 14.15 15.28 70.55 90.90 87.64]	34.92	
	12 : [5.14 14.58 15.67 114.09 89.47 95.63]	25.53	
	16 : [4.97 14.04 14.91 69.14 85.24 88.08]	43.55	
	35 : [5.02 14.05 15.68 112.54 93.18 91.99]	30.16	
	37 : [5.57 14.97 16.74 114.79 102.06 84.89]	22.44	
	46 : [5.30 15.35 17.07 105.90 93.19 94.77]	26.47	
	50 : [5.29 13.52 15.33 66.19 87.58 81.43]	60.33	
5	13 : [20.14 20.36 24.79 96.29 73.85 70.27]	47.80	Unclassified
	39 : [18.79 21.92 25.65 88.53 97.53 114.22]	58.45	
6	15 : [0.01 12.22 15.30 66.74 89.94 89.85]	30.47	Unclassified
7	22 : [14.46 16.59 18.80 59.27 68.99 79.43]	44.20	Unclassified
	44 : [14.20 17.88 18.42 111.72 107.70 92.18]	40.37	
8	24 : [14.63 15.24 20.86 94.56 86.30 56.49]	20.36	Unclassified
	27 : [14.13 14.43 19.86 82.43 69.88 62.55]	38.45	
	32 : [13.52 15.50 21.42 100.51 104.71 114.75]	68.51	
	33 : [13.98 14.52 19.29 83.77 69.05 63.05]	33.70	
	58 : [13.91 14.52 19.96 82.31 61.71 63.71]	23.64	
9	26 : [8.35 11.33 11.66 71.60 73.41 83.14]	43.71	Unclassified
	41 : [8.67 11.35 13.37 83.74 76.60 84.45]	39.46	
10	29 : [7.41 12.04 64.22 147.04 75.44 113.72]	22.77	Unclassified
11	30 : [5.12 5.79 5.86 87.51 89.23 65.10]	34.97	Unclassified

	47 : [3.85 4.19 4.22 60.64 85.22 61.93]	23.09	
	54 : [5.20 5.21 5.56 87.08 87.11 66.27]	30.52	
12	34 : [5.22 25.00 26.77 115.78 96.07 92.99]	35.41	Unclassified
13	36 : [14.21 15.79 28.12 67.22 76.55 64.11]	28.49	Unclassified
	59 : [14.59 14.65 27.21 94.49 83.33 63.57]	31.12	
14	38 : [5.42 7.72 15.38 80.17 80.53 70.60]	31.28	Unclassified
	48 : [5.95 7.32 13.30 92.78 95.31 112.25]	25.43	
15	52 : [14.21 14.95 39.12 76.89 88.34 64.27]	20.87	Unclassified
16	55 : [14.11 15.11 55.55 84.82 84.49 62.29]	33.81	Unclassified
17	60 : [14.22 14.91 24.28 80.09 69.04 62.20]	35.83	Unclassified
18	63 : [15.26 18.61 26.54 80.57 93.69 81.96]	47.91	Unclassified

The unclassified unit cells mainly belong to data sets of multiple lattices or bad data quality, resulting in unit cell parameters with large deviations or are wrong.

Table S5 Crystallographic and experimental parameters of the calcined Product B.

Parameters	**IWV**	***CTH**
Phase composition (%)	67	33
Chemical Formula[a]	$[Si_{136}Ge_{16}O_{304}]$	$[Si_{28}Ge_4O_{64}]$
Space group	$Fmmm$	$Cmm2$
a (Å)	13.7812(4)	13.7200(5)
b (Å)	25.2863(10)	27.5719(13)
c (Å)	28.1442(10)	5.0376(3)
V (Å^3)	9807.6(6)	1905.65(15)
2θ range (°)	1.8 to 35.0	
Wavelength (Å)	0.68950 (X-ray)	
R_I	0.027 (**IWV**), 0.033 (***CTH**)	
R_{wp}	0.169	
R_{exp}	0.116	
GoF	1.45	
Observations	9804	
Contributing reflections	1214 (**IWV**), 529 (***CTH**)	
Total parameters	152	
Restraints	84 (**IWV**), 74 (***CTH**)	

[a] The main purpose of the Rietveld refinement conducted here is to determine the phase composition of Product B. Al atoms were not included during the refinement as it is very difficult to distinguish Si and Al using the SPXRD data. Ge atoms were included in refinement as the ^{19}F solid-state NMR spectrum shows that significant Ge atoms are located in the *d*4*r* units (Figure S19). Meanwhile, the SPXRD data is possible to tell the difference between Si and Ge atoms.

Table S6 The reported expensive, bulky, and complex OSDAs that are used to synthesize **SFE**, **IWV**, and ***CTH**.

Zeolite	OSDA	Reference
SFE	 *N*,*N*-Diethyldecahydroquinolinium	16,17
IWV	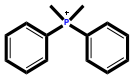 dimethyldiphenylphosphonium 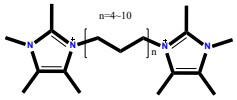 diquaternary imidazolium	18,19
***CTH**	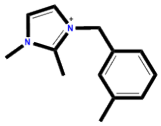 1,2-Dimethyl-3-(3,5-dimethylbenzyl)imidazolium 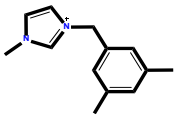 1-Methyl-3-(3,5-dimethylbenzyl)imidazolium	20

Table S7. Textural properties of **MOR**, **SFE**, and Product B

Sample	Si/Ge[a]	Si/B[a]	Si/Al[a]	S_{BET}[b] (m^2/g)	S_{micro}[b] (m^2/g)	S_{ext}[b] (m^2/g)	V_{micro}[b] (cm^3/g)
MOR	∞	∞	18	373	348	25	0.16
SFE[c]	∞	84	57	375	241	134	0.11
Product B	6	∞	17	427	368	59	0.17

[a] analyzed by ICP. [b] analyzed by BET and t-plot methods.

[c] SFE zeolite was firstly synthesized in borogermanosilicate form using DMAP as OSDA. Its aluminoborosilicate form was prepared later by optimizing the synthesis condition.[12]

Table S8. Catalytic results of IPN disproportionation over **SFE**, **MOR**, and Product B catalysts (reaction time: 6h, temperature: 250°C).

Sample	IPN conv. (%)[a]	Distribution of diisopropylnaphthalenes (DIPN) (mol %)					β,β-selectivity (mol %)[b]	2,6-DIPN/ 2,7-DIPN
		1,3-DIPN	1,7-DIPN	2,6-DIPN	2,7-DIPN	Other		
MOR	15.3	11.1	5.2	45.5	29.8	8.3	75.3	1.5
SFE	6.4	21.8	13.5	37.9	17.3	9.5	55.2	2.2
Product B	32.3	4.8	6.6	42.2	37.6	8.8	79.8	1.1

[a] IPN=isopropylnaphthalene. [b] *β,β*-selectivity=(2,6-DIPN+2,7-DIPN)/DIPN*100%.

References

1. Moliner, M., Rey, F. & Corma, A. Towards the Rational Design of Efficient Organic Structure-Directing Agents for Zeolite Synthesis. *Angew. Chem. Int. Ed.* **52**, 13880-13889 (2013).
2. Gómez-Hortigüela, L. & Camblor, M. Á. Introduction to the Zeolite Structure-Directing Phenomenon by Organic Species: General Aspects. in *Insights into the Chemistry of Organic Structure-Directing Agents in the Synthesis of Zeolitic Materials*, 1-41 (Springer International Publishing, 2018).
3. Zones, S. I. Translating new materials discoveries in zeolite research to commercial manufacture. *Microporous Mesoporous Mater.* **144**, 1-8 (2011).
4. Wragg, D. S., Morris, R. E. & Burton, A. W. Pure Silica Zeolite-type Frameworks: A Structural Analysis. *Chem. Mater.* **20**, 1561-1570 (2008).
5. Sastre, G. & Corma, A. Rings and Strain in Pure Silica Zeolites. *J. Phys. Chem. B* **110**, 17949-17959 (2006).
6. Li, J., Corma, A. & Yu, J. Synthesis of new zeolite structures. *Chem. Soc. Rev.* **44**, 7112-7127 (2015).
7. Jiang, J. *et al.* Investigation of Extra-Large Pore Zeolite Synthesis by a High-Throughput Approach. *Chem. Mater.* **23**, 4709-4715 (2011).
8. Bai, R. *et al.* Simple Quaternary Ammonium Cations-Templated Syntheses of Extra-Large Pore Germanosilicate Zeolites. *Chem. Mater.* **28**, 6455-6458 (2016).
9. Wang, B., Zou, X. & Smeets, S. Automated serial rotation electron diffraction combined with cluster analysis: an efficient multi-crystal workflow for structure determination. *IUCrJ* **6**, 854-867 (2019).
10. Cichocka, M. O., Ångström, J., Wang, B., Zou, X. & Smeets, S. High-throughput continuous rotation electron diffraction data acquisition via software automation. *J Appl Cryst.* **51**, 1652-1661 (2018).
11. Kabsch, W. XDS. *Acta Cryst. D,* **66**, 125-132 (2010).
12. Luo, Y. *et al.* A Facile and Green Method for the Synthesis of SFE Borosilicate Zeolite and Its Heteroatom-Substituted Analogues with Promising Catalytic Performances. *Chem. Eur. J.* **24**, 306-311 (2018).
13. Brzozowski, R. & Skupiński, W. Disproportionation of isopropylnaphthalene on zeolite catalysts. *J. Catal.* **220**, 13-22 (2003).
14. Brzozowski, R. Isomerization of diisopropylnaphthalenes on wide-pore zeolites. *J. Catal.* **232**, 366-377 (2005).
15. Foadi, J. *et al.* Clustering procedures for the optimal selection of data sets from multiple crystals in macromolecular crystallography. *Acta Cryst. D* **69**, 1617-1632 (2013).
16. Wagner, P. *et al.* Electron Diffraction Structure Solution of a Nanocrystalline Zeolite at Atomic Resolution. *J. Phys. Chem. B* **103**, 8245-8250 (1999).
17. Lee, G. S. *et al.* Organocations in Zeolite Synthesis: Fused Bicyclo [*l.m.0*] Cations and the Discovery of Zeolite SSZ-48. *J. Am. Chem. Soc.* **124**, 7024-7034 (2002).
18. Dorset, D. L. *et al.* P-Derived Organic Cations as Structure-Directing Agents: Synthesis of a High-Silica Zeolite (ITQ-27) with a Two-Dimensional 12-Ring Channel System. *J. Am. Chem. Soc.* **128**, 8862-8867 (2006).
19. Schmidt, J. E., Chen, C.-Y., Brand, S. K., Zones, S. I. & Davis, M. E. Facile Synthesis, Characterization, and Catalytic Behavior of a Large-Pore Zeolite with the IWV Framework. *Chem. Eur. J.* **22**, 4022-4029 (2016).

20. Kang, J. H. *et al.* Synthesis and Characterization of CIT-13, a Germanosilicate Molecular Sieve with Extra-Large Pore Openings. *Chem. Mater.* **28**, 6250-6259 (2016).